Lifetime seismic performance of concrete bridges exposed to corrosion

Fabio Biondini[a], Elena Camnasio[a]* and Alessandro Palermo[b]

[a]*Department of Civil and Environmental Engineering, Politecnico di Milano, Milan, Italy;* [b]*Department of Civil and Natural Resources Engineering, University of Canterbury, Christchurch, New Zealand*

(*Received 3 November 2011; final version received 22 June 2012; accepted 7 December 2012*)

Introduction

Concrete structures exposed to aggressive environments are subjected to lifetime degradation induced by the kinetic process of diffusion of chemical components, such as sulphates and chlorides, driven by concentration gradients inside the material volume (Glicksman, 2000). Sulphates contained in soil or water can contaminate the cement paste causing a progressive loss of concrete strength. Chlorides beyond a threshold value in carbonated concrete can lead to the corrosion of reinforcing steel (Bertolini, Elsener, Pedeferri, & Polder, 2004). Chlorides are critical in a marine environment, where they diffuse into concrete as airborne chlorides and/or by direct contact with seawater, especially in the tidal and splash zone, but they can also come from the application of deicing salts on bridge decks (CEB, 1992).

In general, for concrete structures, damage scenarios are more critical for bridges than for buildings, since usually the entire structure is directly exposed to the aggressive atmosphere without protection. The influence of corrosion on the traffic load capacity of bridge systems has been widely studied (Biondini & Frangopol, 2008a, 2008b; Estes & Frangopol, 2001; Val, Stewart, & Melchers, 1998), showing that the deterioration of performance resulting from reinforcement corrosion could have a significant effect on both serviceability and ultimate limit states. Therefore, durability issues should be properly considered in the assessment of bridge system reliability (Akiyama, Frangopol, & Suzuki, 2011).

Recent studies (Akiyama & Frangopol, 2010; Akiyama, Frangopol, & Matsuzaki, 2011; Akiyama, Matsuzaki, Dang, & Suzuki, 2012; Alipour, Shafei, & Shinozuka, 2013; Biondini, Camnasio, & Palermo, 2010; Choe, Gardoni, Rosowsky, & Haukaas, 2008, 2009; Ghosh & Padgett, 2009, 2010; Kumar, Gardoni, & Sanchez-Silva, 2009) show that the effect of corrosion becomes even more relevant if the bridges are subjected to seismic loading, since the transversal load-carrying capacity can be significantly affected by corrosion of both longitudinal and transversal reinforcement. In particular, corrosion of stirrups can become critical in those zones where prescribed levels of confinement and shear strength are needed for a proper performance of concrete members, such as the bottom and/or the top of bridge piers where a plastic hinge is expected to occur under seismic load (Oyado, Saito, Yasojima, Kanakubo, & Yamamoto, 2007). In fact, the dissipative capacity of these critical zones, which the current seismic design philosophies rely on, may vary over time, due to the lifetime reduction of both strength and displacement ductility caused by the degradation process of the materials.

Consequently, the collapse mechanism and the corresponding ductility capacity of the bridge depend on

*Corresponding author. Email: elena.camnasio@mail.polimi.it

both environmental exposure and structural ageing (Biondini & Frangopol, 2008a; Biondini, Palermo, & Toniolo, 2011). However, while the strength reduction of concrete members suffering corrosion can be directly related to the reduction of the steel bars area, the effects on stiffness and ductility of the overall structure are associated with more complex mechanisms, including lack of confinement due to corrosion of transversal reinforcement (Oyado et al., 2007) and bond deterioration between steel reinforcing and surrounding concrete (Ou, Wang, Tsai, Chang, & Lee, 2010). Moreover, the situation can be further complicated if different geometrical parameters as distribution of bridge pier heights and deck stiffness are considered, since these aspects can considerably affect the overall seismic performance of bridge systems (Palermo & Pampanin, 2008).

To afford this problem, a probabilistic approach to predict the lifetime seismic performance of concrete bridges exposed to aggressive environments is presented in this paper. The proposed approach is based on a general methodology for the lifetime assessment of concrete structures proposed in Biondini, Bontempi, Frangopol, and Malerba (2004), Biondini, Bontempi, Frangopol, and Malerba (2006) and in Biondini and Frangopol (2008a), and extended to account for seismic performance in Biondini et al. (2011). The study presented in Biondini et al. (2011) was based on deterministic nonlinear static (push-over) analyses aimed to investigate the lifetime evolution of the seismic capacity of concrete structures. In this paper, the seismic capacity of bridge structures is compared with the seismic demand over lifetime in probabilistic terms by considering the uncertainties involved in the problem. In this way, the design target levels are related to the lifetime evolution of the seismic performance within a life cycle-oriented performance-based design approach. Moreover, in order to investigate the effects of damage on the actual seismic behaviour and to clarify the interaction between seismic and environmental hazards, nonlinear dynamic analyses under prescribed ground motions are carried out over the structural lifetime.

The proposed procedure is applied to a concrete continuous bridge with box cross-section piers exposed to corrosion. The time-variant behaviour of critical cross-sections at the base of the bridge piers is evaluated in terms of bending moment versus curvature relationships, accounting for the degradation of both concrete and steel. The inherent randomness of the diffusion process, as well as the material and geometrical uncertainties, which affect the structural response, is taken into account by means of Monte Carlo simulation. A time-variant probabilistic analysis is carried out at the cross-sectional level to investigate the time evolution of performance indicators such as bending resistance and curvature ductility. The lifetime probabilistic seismic performance of the bridge structural system is therefore obtained by means of time-variant nonlinear static and dynamic analyses.

Seismic strength versus displacement ductility is investigated by means of push-over analyses with reference to limit states related to damage thresholds and structural collapse. The evolution of the force–displacement curves of the structure is evaluated, showing that the residual capacity of carrying transversal actions, such as those associated with seismic events, depends on the age of the structure. Based on these results, the design maximum peak ground acceleration can be determined by prescribing a design target level in terms of maximum displacement or drift, in order to ensure an acceptable seismic performance of the structure over lifetime. Time-histories analyses are finally carried out to validate the results of the push-over analyses and to confirm that the combination of both seismic hazard, considered as increasing seismic intensity levels, and aggressiveness of environmental exposure, related to material degradation phenomena, may affect the overall lifetime seismic performance of the bridge structure.

Time-variant performance of concrete cross-sections

In order to investigate the seismic performance of ageing concrete bridges, the evaluation of the lifetime evolution of cross-sectional performance indicators, such as ultimate moment M_{ult} and curvature ductility μ_χ, is performed in probabilistic terms by considering the randomness of both the diffusion process and the main parameters of the structure at the cross-sectional level, i.e. material properties, geometrical dimensions, area and location of the reinforcing bars.

The diffusion process

Since most observations indicate that the transportation of chlorides in concrete is diffusion controlled (Bertolini et al., 2004), the diffusive process leading to corrosion is described by using the following limit state equation based on Fick's one-dimensional (1D) model (*fib*, 2006):

$$\begin{aligned} C(x=c,t) &= C_0 + (C_{\text{S},\Delta x} - C_0)\cdot\left[1 - \operatorname{erf}\frac{c-\Delta x}{2\cdot\sqrt{D_{\text{app},C}\cdot t}}\right] \\ &= C_{\text{crit}}, \end{aligned} \tag{1}$$

where the actual chloride concentration $C(x = c,\ t)$ at the depth of the concrete cover c at time t is compared to the critical chloride concentration C_{crit} which defines the initiation of the corrosion process; C_0 is the initial chloride content in the cement paste; Δx is the depth of the

Table 1. Probability distributions and their parameters of the random variables involved in the diffusion process (*fib*, 2006).

Random variable	Distribution type	μ	σ
Concrete cover, c (mm)	Normal[a]	40	8
Aging coefficient, a (–)	Beta ($b_{min} = 0.0$; $b_{max} = 1.0$)[b]	0.3	0.12
Chloride content at depth Δx, $C_{s,\Delta x}$ (wt.%/cem)	Normal[a]	3	0.30μ
Chloride migration coefficient, $D_{RCM,0}$ (m^2/s)	Normal[a]	15.8×10^{-12}	0.20μ
Critical chloride content, C_{crit} (wt.%/cem)	Beta ($b_{min} = 0.2$; $b_{max} = 2.0$)[b]	0.6	0.15

[a] Truncated distributions with non negative outcomes.
[b] b_{min} = lower bound and b_{max} = upper bound of beta distributions.
[c] For spray conditions (spray road environment, spray marine environment).

convection zone, i.e. the concrete layer up to which the process of chloride penetration differs from Fick's model; $C_{S,\Delta x}$ is the chloride content at depth Δx and time t and $D_{app,C}$ is the apparent coefficient of chloride diffusion, which is evaluated as follows (*fib*, 2006):

$$D_{app,C}(t) = D_{RCM,0} \cdot A(t), \tag{2}$$

where $D_{RCM,0}$ is the chloride migration coefficient and $A(t)$ is a function considering 'ageing' (*fib*, 2006):

$$A(t) = \left(\frac{t_0}{t}\right)^a, \tag{3}$$

where $t_0 = 28$ days is the reference initial time and a is an ageing coefficient depending on the cement type.

The diffusion process is described in probabilistic terms by assuming the main parameters of the problem as random variables with the distribution type, mean μ and standard deviation σ listed in Table 1 (*fib*, 2006). In this model, $C_0 = 0$ and $\Delta x = 0$ are also assumed. The probability density functions (PDFs) of chloride concentration obtained from a Monte Carlo simulation with a sample size of 50,000 realisations are shown in Figure 1, with reference to a cover depth $c = 40$ mm and time steps $\Delta t = 10$ years for a lifetime of 50 years.

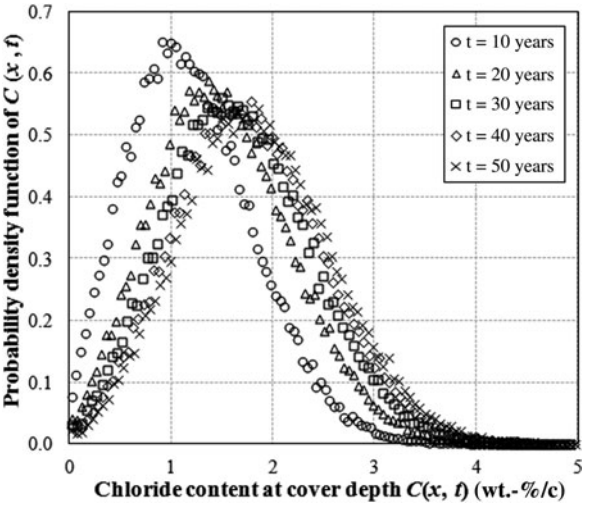

Figure 1. PDFs of chloride concentration in concrete $C(x, t)$ at cover depth $x = c = 40$ mm and time steps $\Delta t = 10$ years for a 50-year lifetime.

Corrosion initiation time

In general, the deterioration process includes corrosion initiation and corrosion propagation. The corrosion initiation time t_i represents the period during which the aggressive agents penetrate by means of diffusion into the protective concrete cover or by direct ingress through cracks induced by loading exceeding the cracking capacity of the section and by shrinkage, among others. When the threshold level of concentration C_{crit} is reached at the steel bar surface, the corrosion propagation starts (Alonso, Andrade, Castellote, & Castro, 2000; Alonso, Castellote, & Andrade, 2002; Glass & Buenfeld, 1997; Hope & Alan, 1987). With reference to the Fick's 1D model of diffusion, the initiation time t_i for the propagation of steel bar corrosion is evaluated as follows:

$$t_i = \frac{(c - \Delta x)^2}{4 \cdot D_c} \cdot \left[\text{erf}^{-1}\left(\frac{C_{S,\Delta x} - C_{crit}}{C_{S,\Delta x} - C_0}\right)\right]^{-2}, \tag{4}$$

where the approximation $D_c \cong D_{RCM,0}$ is assumed for short exposure time intervals.

Based on the assumed modelling of random variables, the PDF obtained for the corrosion initiation time t_i is shown in Figure 2. A lognormal distribution with mean $\mu = 1.19$ years and standard deviation $\sigma = 0.87$ years appears to be a good estimate of the actual distribution for the corrosion initiation time $t_i \leq 50$ years (Figure 2, continuous line). It is worth noting that the relatively short initiation time is related to the severe conditions assumed for exposure, chloride content and diffusion coefficient of concrete.

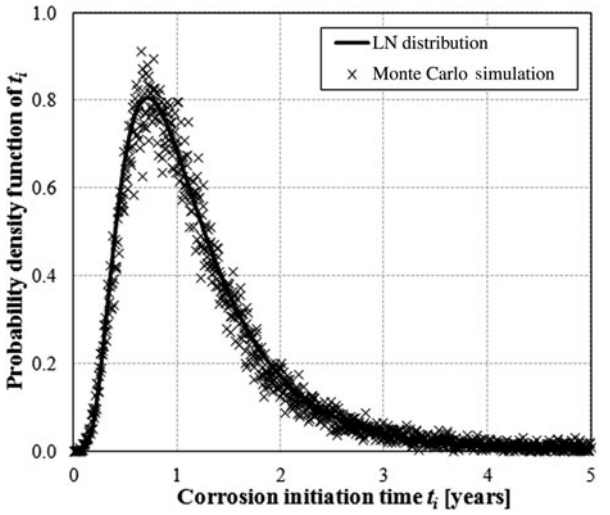

Figure 2. PDF of corrosion initiation time t_i.

Damage modelling

Reduction in the cross-section area of steel bars

The chloride attack induces a corrosion process with reduction in the area of steel reinforcing bars. The corrosion penetration P_x is evaluated as follows:

$$P_x = \int_{t_i}^{t_i+t_p} r_{corr}\, dt, \tag{5}$$

where r_{corr} is the corrosion rate and $t_p = (t - t_i)$ is the propagation time. Considering uniform corrosion, the reduction in the diameter $\Phi(t)$ of a corroding reinforcing bar at time t can be estimated as follows (Berto, Vitaliani, Saetta, & Simioni, 2009):

$$\Phi(t) = \Phi_0 - 2P_x \tag{6}$$

or

$$\Phi(t) = \Phi_0(1 - \delta), \tag{7}$$

where $\Phi_0 = \Phi(0)$ and $\delta \in [0; 1]$ is a dimensionless corrosion penetration index:

$$\delta = \frac{2P_x}{\Phi_0}. \tag{8}$$

The area A_s of a corroded steel bar can be represented as a function of the corrosion index as follows (Biondini et al., 2004):

$$A_s(\delta) = [1 - \delta_s(\delta)]A_{s0}, \tag{9}$$

where $A_{s0} = \pi\Phi_0^2/4$ is the area of the undamaged steel bar and $\delta_s = \delta_s(\delta)$ is a dimensionless damage function which provides a measure of cross-section reduction in the range [0; 1].

On the basis of correlations between chloride content and corrosion current density in concrete (Bertolini et al., 2004; Liu & Weyers, 1998; Pastore & Pedeferri, 1994; Thoft-Christensen, 1998), a linear relationship between rate of corrosion r_{corr}, in the range 0–200 μm/year, and chloride content C, in the range 0–3%, is approximately assumed for structures exposed to severe environmental conditions (Biondini et al., 2004, 2006). The dependency of the corrosion initiation time on different parameters, such as concrete cover thickness or quality and type of cement, has been widely researched and modelled (Browne, Geoghegan, & Baker, 1983; Hamada, 1968). On the contrary, the parameters related to the propagation period are still affected by greater uncertainties. In particular, the corrosion rate can hardly be assessed reliably, since it depends on several parameters related to both environmental conditions and characteristics of concrete. For this reason, the few available experimental data cannot be representative of a wide range of corrosion scenarios. In addition, it is difficult to establish which parameters can effectively represent the level of concrete deterioration, i.e. steel section loss, cracking and concrete spalling, among others (Andrade & Alonso, 1994; Andrade, Alonso, & Gonzalez, 1990). This topic should therefore be further investigated in order to obtain reliable long-term concrete durability prediction.

Reduction in ductility of reinforcing steel

The corrosion process causes not only a reduction in the steel mass, but also a loss of ductility of the material that can lead to brittle failures of concrete members (Coronelli & Gambarova, 2004; Stewart, 2009). Tensile tests on corroded bars show that the steel behaviour may become brittle even for a quite limited (about 13%) mass loss (Almusallam, 2001). The ductility reduction can be considered as a function of mass loss, according to several formulas calibrated on experimental data obtained from corrosion tests on concrete specimens in both artificial and natural conditions (Apostolopoulos & Papadakis, 2008; Kobayashi, 2006).

If uniform corrosion is considered, the cross-section reduction δ_s of the steel bar depends on the corrosion penetration index δ as follows (Biondini, 2011):

$$\delta_s = \delta(2 - \delta). \tag{10}$$

Therefore, the steel ultimate strain $\varepsilon_{su}(t)$ can be expressed as follows (Biondini & Vergani, 2012; Vergani, 2010):

$$\varepsilon_{su}(t) = \begin{cases} \varepsilon_{su0} & 0 \le \delta_s \le 0.016 \\ 0.1521 \cdot \delta_s^{-0.4583}\varepsilon_{su0} & 0.016 < \delta_s \le 1 \end{cases} \tag{11}$$

in which ε_{su0} is the nominal value of the steel ultimate strain.

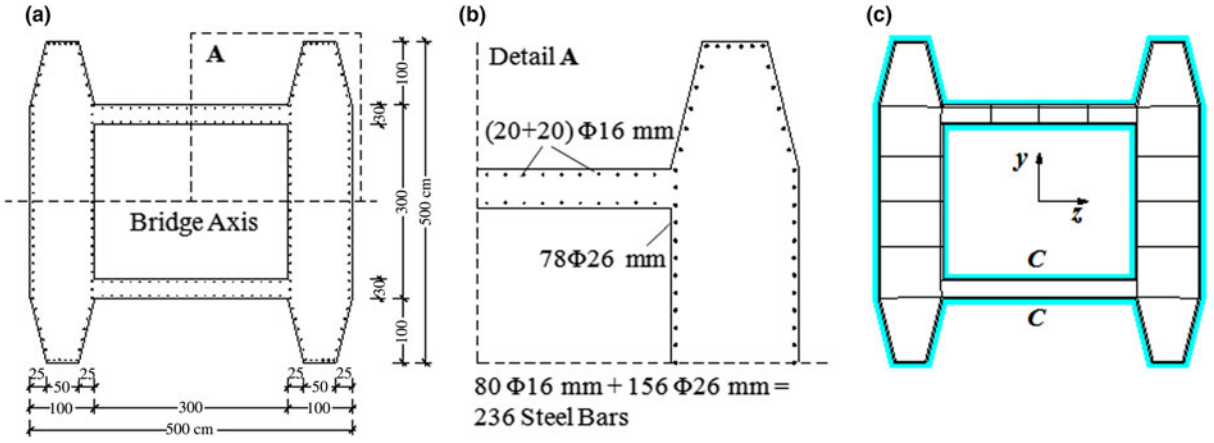

Figure 3. Pier cross-section: (a) geometrical dimensions; (b) reinforcement layout; (c) model of the cross-section and location of the aggressive agent.

Effects of corrosion on concrete

Since the formation of oxidation products may lead to propagation of longitudinal cracks and concrete cover spalling, the local deterioration of concrete has to be taken into account to properly estimate the residual strength of the material during lifetime. The reduced concrete strength $f_c(t)$ can be evaluated as follows (Coronelli & Gambarova, 2004):

$$f_c(t) = \frac{f_{c0}}{1 + \kappa[\varepsilon_\perp(t)/\varepsilon_{c0}]}, \tag{12}$$

where κ is a coefficient related to bar diameter and roughness ($\kappa = 0.1$ for medium-diameter ribbed bars), ε_{c0} is the strain at peak stress in compression and $\varepsilon_\perp(t)$ is the transversal strain at time t. The evaluation of the transversal strain $\varepsilon_\perp(t)$ is based on the following relationship:

$$\varepsilon_\perp(t) = \frac{n_{bars} w}{b_i}, \tag{13}$$

where b_i is the width of the undamaged cross-section, n_{bars} is the number of steel bars and w is the mean crack opening for each bar. Several studies investigated the relationship between the amount of corrosion and cover cracking (Alonso, Andrade, Rodriguez, & Diez, 1998; Zhang, Castel, & François, 2009). The following empirical model is proposed in Vidal, Castel, and Francois (2004):

$$w = \kappa_w(\delta_s - \delta_{s0})A_{s0}, \tag{14}$$

where $\kappa_w = 0.0575\,\text{mm}^{-1}$, δ_s is the damage function and δ_{s0} is the amount of steel damage necessary for cracking initiation. For uniform corrosion, the damage threshold δ_{s0} is evaluated as follows (Vidal et al., 2004):

$$\delta_{s0} = 1 - \left[1 - \frac{1}{\Phi_0}\left(7.53 + 9.32\frac{c}{\Phi_0}\right) \times 10^{-3}\right]^2, \tag{15}$$

where the bar diameter $\Phi_0 = \Phi(0)$ and the concrete cover c are given in millimeters. The reduction in concrete strength is generally applied to the entire concrete cover. However, the longitudinal crack pattern strongly depends on the arrangements of the reinforcing bars. The propagation of corrosion-induced cracking should be therefore limited to the zone adjacent to the reinforcing bars to model the damage phenomena properly (Biondini & Vergani, 2012; Vergani, 2010).

Case study. Box cross-section of a bridge pier

The case study of a bridge pier with the box cross-section shown in Figure 3(a),(b), which is typically adopted for medium/high bridge piers, is considered here in order to show the effectiveness of the proposed procedure. The aim is to investigate the evolution of performance indicators such as ultimate moment M_{ult} and curvature ductility μ_χ at the cross-sectional level, which vary over lifetime due to damage. The pier cross-section has main nominal dimensions $d_y = d_z = 5.00$ m; the concrete cross-section is reinforced with $80 + 156 = 236$ steel bars having nominal diameters $\Phi_{nom} = 16$ mm and $\Phi_{nom} = 26$ mm, respectively, with a concrete cover $c = 40$ mm. A nominal compression strength of the concrete $f_c = 30$ MPa and a nominal yielding strength of the steel $f_{sy} = 500$ MPa are assumed. Strain values $\varepsilon_{c0} = 0.22\%$ and $\varepsilon_{cu} = 0.35\%$ for concrete in compression and $\varepsilon_{su0} = 5.00\%$ for steel are also assumed.

The column cross-section is considered exposed to the diffusive attack of chlorides along both the external and internal perimeters with $C_{s,\Delta x}(t) = C$ (Figure 3(c)).

Table 2. Bridge pier cross-section data: probability distributions and their parameters.

Random variable	Distribution type	μ	σ
Concrete strength, f_c (MPa)	Lognormal	$f_{c,nom}$	5
Steel strength, f_{sy} (MPa)	Lognormal	$f_{sy,nom}$	30
Coordinates of the nodal points, (y_i,z_i) (mm)	Normal	$(y_i,z_i)_{nom}$	5
Coordinates of the steel bars, (y_m,z_m) (mm)	Normal	$(y_m,z_m)_{nom}$	5
Diameter of the steel bars, Φ (mm)	Normal[a]	Φ_{nom}	0.10μ

[a] Truncated distribution with non negative outcomes.

The hollow core is exposed to the atmosphere as the external surface since this type of piers is not hermetically closed over the whole height, having openings particularly in the top part. The 1D Fick's law of diffusion is applied in the normal direction to each side of the cross-section boundary. The interaction of the diffusion process from more than one side of the cross-section is neglected (Berto et al., 2009), since the effects of 2D patterns of diffusion are relevant only for the few steel bars placed close to the corners of the cross-section. The reduction of strength in concrete is applied to the entire concrete cover.

Corrosion of steel bars and damage of concrete

The material strengths and the diameter of the steel bars are assumed as random variables with the probability distributions, mean μ and standard deviation σ listed in Table 2. According to the probability distribution of the random variables affecting the diffusion process (Table 1) and considering the corrosion initiation time shown in Figure 2, the reduction of the steel bar diameters in the cross-section, i.e. $\Phi_{nom} = 16$ mm and $\Phi_{nom} = 26$ mm, is evaluated over a lifetime of 50 years with $\Delta t = 10$ years. The time-variant mean values μ of steel bar diameter ratio $\Phi(t)/\Phi_0$ and the corresponding standard deviations σ are shown in Figure 4(a),(b). The scatter around the mean increases during lifetime due to the increasing effects of the uncertainties related to the degradation phenomena, which are added to the material and geometrical inherent variability. It is noted that the effects of steel reinforcement corrosion are more significant for small bar diameters, as expected, since the percentage of bar diameter loss is greater. Consequently, in a corroding structure few large diameter bars are apparently safer than a higher number of small diameter bars (Andrade et al., 1990). However, the loss of steel mass should be compared with the other effects of corrosion to better clarify the role of the bar diameter on the lifetime deterioration process.

The evolution of the damage function $\delta_s(t)$, which has a direct dependency on the reduction of the bar diameter, allows to evaluate the ultimate deformation of steel $\varepsilon_{su}(t)$ and the strength of concrete cover $f_c(t)$ during lifetime, as shown in Figure 5 for (a) $\Phi_{nom} = 16$ mm and

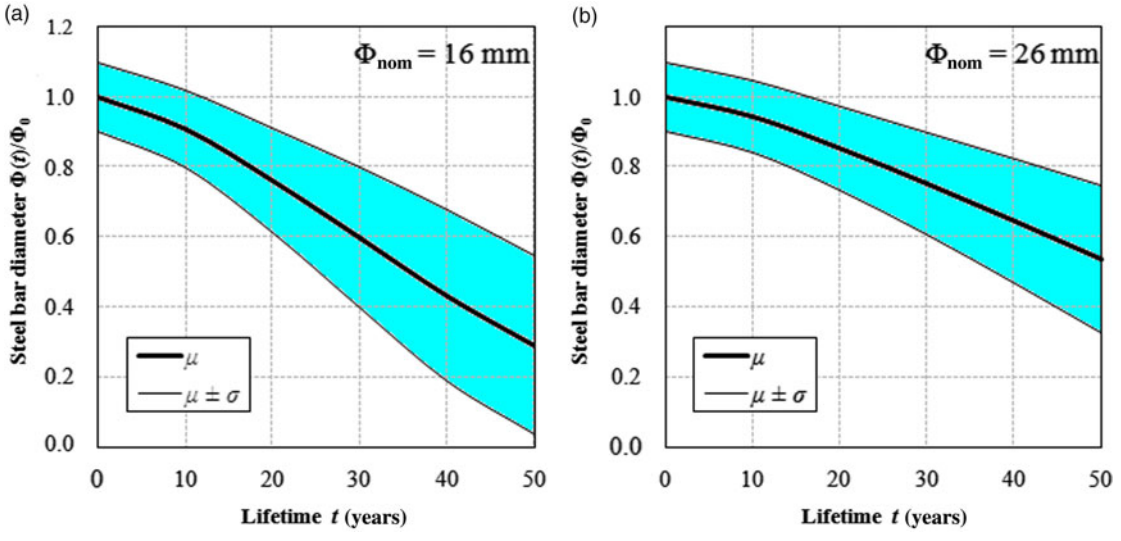

Figure 4. Time evolution of steel bar diameter $\Phi(t)$ for (a) $\Phi_{nom} = 16$ mm and (b) $\Phi_{nom} = 26$ mm (mean μ and standard deviation σ from the mean).

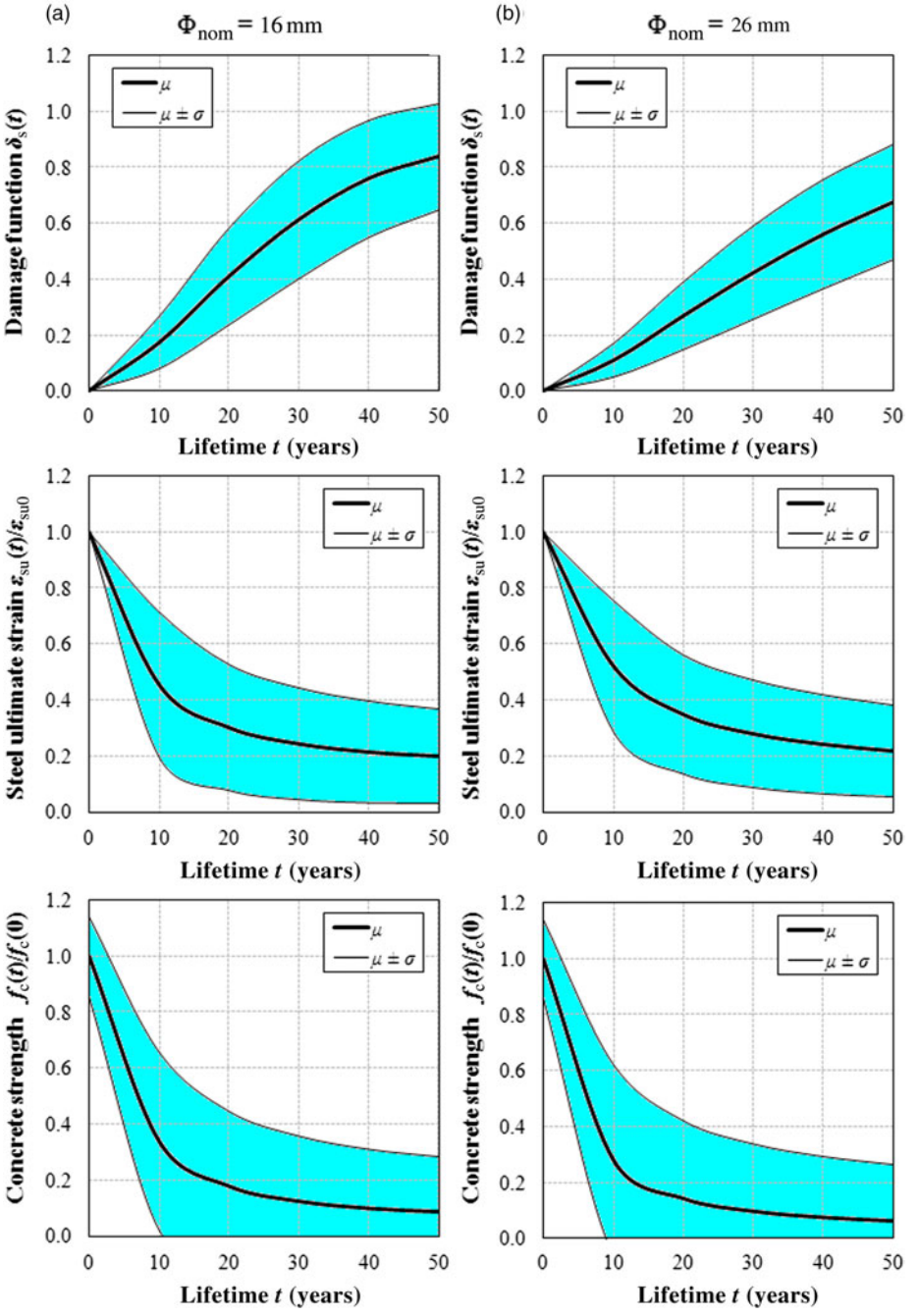

Figure 5. Time evolution of the damage function $\delta_s(t)$, steel ultimate strain $\varepsilon_{su}(t)$ and concrete strength $f_c(t)$ for (a) $\Phi_{nom} = 16$ mm and (b) $\Phi_{nom} = 26$ mm (mean μ and standard deviation σ from the mean).

(b) $\Phi_{nom} = 26$ mm. These results indicate that the influence of the size of steel bars on the lifetime reduction of both steel ultimate strain and concrete strength is less significant compared with the loss of steel mass (Figure 5). However, it is worth noting that the reduction of concrete strength is greater for $\Phi_{nom} = 26$ mm, since the width of cracks increases with larger diameters. With this regard, small bar diameters seem therefore preferable than large bar diameters to avoid splitting cracks and spalling of concrete cover and, in this way, to limit the chloride ingress into concrete.

The validity of the simulation results with respect to the sample size n is highlighted in Figure 6, with reference to the evolution of the steel bar diameters $\Phi_{nom} = 16$ mm and $\Phi_{nom} = 26$ mm. The evolution of both mean μ and standard deviation σ towards stable values after $n = 50{,}000$ realisations proves the accuracy of the simulation process.

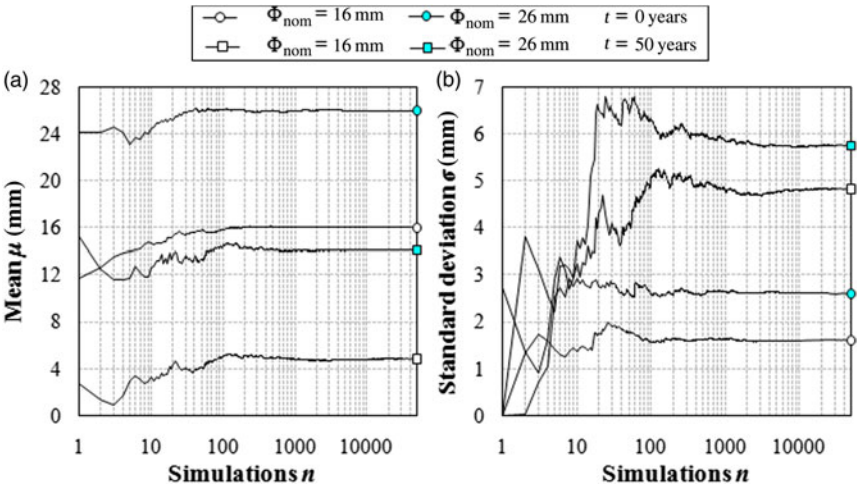

Figure 6. Evolution during the simulation process of (a) mean μ and (b) standard deviation σ of steel bar diameters $\Phi_{nom} = 16$ mm and $\Phi_{nom} = 26$ mm at time $t = 0$ and $t = 50$ years.

Lifetime moment-curvature relationships

The structural analysis of the cross-section assumes the linearity of concrete strain field and neglects the bond slip of reinforcement. Based on these hypotheses, the vectors $\mathbf{r} = \mathbf{r}(t) = [N\, M_z\, M_y]^T$ of the stress resultants (axial force N and bending moments M_z and M_y) and of the global strains $\mathbf{e} = \mathbf{e}(t) = [\varepsilon_0\, \chi_z\, \chi_y]^T$ (axial elongation ε_0 and bending curvatures χ_z and χ_y) can be related, at each time instant t, as follows (Malerba, 1998):

$$\mathbf{r}(t) = \mathbf{H}(t)\ \ \mathbf{e}(t), \tag{16}$$

where the stiffness matrix $\mathbf{H}(t) = \mathbf{H}_c(t) + \mathbf{H}_s(t)$ is derived at each time instant by integration over the area of the damaged cross-section by assembling the contributions of concrete $\mathbf{H}_c = \mathbf{H}_c(t)$ and steel $\mathbf{H}_s = \mathbf{H}_s(t)$. Details on the time-variant formulation of the stiffness matrix $\mathbf{H} = \mathbf{H}(t)$ can be found in Biondini et al. (2004, 2006).

The lifetime transversal response of the pier to lateral forces applied normal to the bridge axis is analysed in terms of bending moment-curvature diagram $M_z - \chi_z$ computed by considering an axial load of $N = 25$ MN and $M_y = 0$. The corrosion of the longitudinal steel bars is evaluated according to the proposed model. In this study, the effects of corrosion of the stirrups are not taken into account since confinement is low and it should not affect significantly the bending performance of the cross-section. It is however worth noting that the corrosion of the transversal reinforcement can have significant effects on the seismic response of confined compact cross-section piers (Biondini, Camnasio, & Palermo, 2012; Ou, Tsai, & Chen, 2012; Saito, Oyado, Kanakubo, & Yamamoto, 2007; Yamamoto, Hattori, & Miyagawa, 2006).

The limit state of failure of the cross-section is associated with the reaching of the strain limits of the materials according to the adopted constitutive laws. For concrete, the stress–strain diagram is described by the Saenz's law in compression and by an elastic perfectly plastic model in tension, with the following parameters: compression strength f_c (random variable, see Table 2); tension strength $f_{ct} = 0.25 f_c^{2/3}$ MPa; initial modulus $E_{c0} = 9500 f_c^{1/3}$ MPa; strain limit in tension $\varepsilon_{ctu} = 2 f_{ct}/E_{c0}$. For steel, the stress–strain diagram is described by an elastic perfectly plastic model in both tension and compression with steel strength f_{sy} (random variable, see Table 2) and elastic modulus $E_s = 210$ GPa.

The cross-sectional performance is investigated in probabilistic terms by assuming material strengths, geometrical dimensions, and coordinates of the steel bars as random variables with the distribution type and statistical parameters listed in Table 2. The time evolution of the flexural behaviour of the pier is shown in Figure 7(a) over a lifetime of 50 years with time step $\Delta t = 10$ years. The results refer to bending moment and curvature evaluated considering the sample mean values of the random variables (Table 2, Figures 4 and 5). It can be noticed that the bending capacity of the pier significantly decreases over lifetime, while the curvature capacity shows a different trend. In fact, the ultimate curvature varies depending on the amount of steel in the section, which reduction can actually lead to a more ductile behaviour, as shown after 30 and 40 years of lifetime. Figure 7(b) also shows a four-side stepwise linearisation of the moment-curvature diagram (dotted line) at time $t = 0$. The values of bending moment M_{cr} and curvature χ_{cr} at first cracking of concrete have been reduced with respect to the actual values in order to fit properly the post-cracking stiffness, as shown in Figure 7(b). In this way, also the post-yielding stiffness is estimated more

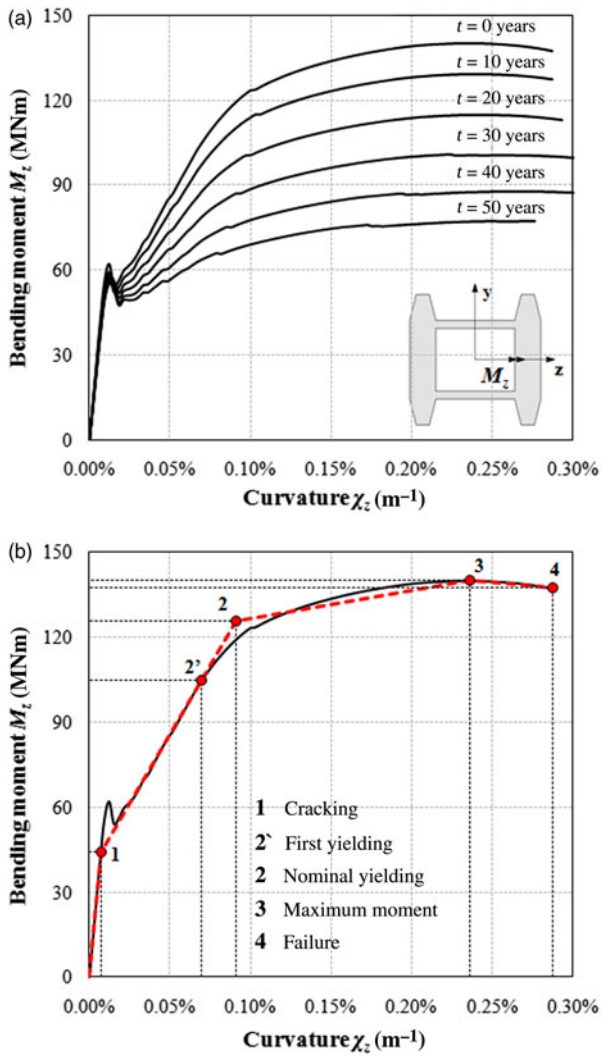

Figure 7. Pier cross-section undergoing corrosion damage: (a) bending moment-curvature diagrams during the first 50 years of lifetime ($N = 25$ MN) according to sample mean values; (b) stepwise linearisation of the bending moment-curvature diagram at time $t = 0$.

accurately. The nominal yielding curvature χ_{yield} is evaluated as follows (Park & Paulay, 1975):

$$\chi_{yield} = \frac{M_{ult}}{M'_y}\chi'_y, \tag{17}$$

where M_{ult} is the moment at failure, M'_y and χ'_y are, respectively, the bending moment and the corresponding curvature evaluated at the first yield of the longitudinal steel bars. The nominal yielding moment of the section M_{yield} is then calculated as the value corresponding to χ_{yield} by linearly interpolating the cracking point and the first yielding point. The maximum bending moment M_{max} and the corresponding curvature χ_{max} are evaluated as the maximum ordinate and corresponding abscissa of the curve. The ultimate properties of the section, i.e. M_{ult} and χ_{ult}, correspond to the achievement of strain limits of concrete or steel.

Lifetime structural performance indicators

Figures 8 and 9 show the probabilistic results obtained by a Monte Carlo simulation based on a sample of 50,000 realisations. The results refer to the time evolution of the bending moments and curvatures associated with the nominal yielding (point 2, Figure 7(b)) and the failure (point 4, Figure 7(b)) of the box cross-section bridge pier. The results are scaled with respect to the mean values of the indicators at time $t = 0$. It can be noticed that, since different uncertainties are associated with each parameter, not only the evolution of the mean μ but also the scatter around the mean is different during 50 years of lifetime.

The ultimate bending moment $M_{ult}(t)$ (Figure 8(b)) and the curvature ductility $\mu_\chi(t) = \chi_{ult}/\chi_{yield}$ (Figure 10) can be assumed as suitable indicators of the seismic performance of the bridge pier. The bending strength and curvature ductility decrease over a lifetime of 50 years of about 40% and 10%, respectively, from the initial values $M_{ult}(0) = 140$ MNm and $\mu_\chi(0) = 3.10$. The bending strength undergoes a monotonic decrease, while the curvature ductility shows a different trend according to the evolution of both the yielding curvature and the ultimate curvature (Figure 9). While the yielding curvature reduces over 50 years of lifetime, the ultimate curvature increases during the first 20 years of lifetime. This is due to the slight decrease of the amount of steel in the concrete cross-section, which leads to a more ductile behaviour. When the steel loss becomes more significant, then the ultimate curvature starts decreasing. This variation in the ultimate curvature trend is hence reflected in the curvature ductility as well.

Experimental accelerated corrosion tests (Oyado et al., 2007) have clarified that the deformation capacity of corroded reinforced concrete elements depends on the reduction in the reinforcing bars area. Moreover, corrosion can eventually cause buckling of the steel bars, thus abruptly reducing the deformation capacity of the section and the corresponding seismic performance of the element. In this work, the buckling failure has not been taken into account, but it is worth noting that in some cases it could change the mechanism of collapse and lead to a brittle structural failure (Akiyama et al., 2011a; Naito, Akiyama, & Suzuki, 2011; Papia, Russo, & Zingone, 1988).

It should also be noticed that while the standard deviation of the results of the yielding curvature remains substantially the same throughout the lifetime, greater uncertainties affect the estimation of the ultimate curvature of a corroded section, as shown in Figure 9. This indicates that the failure mechanism of the section

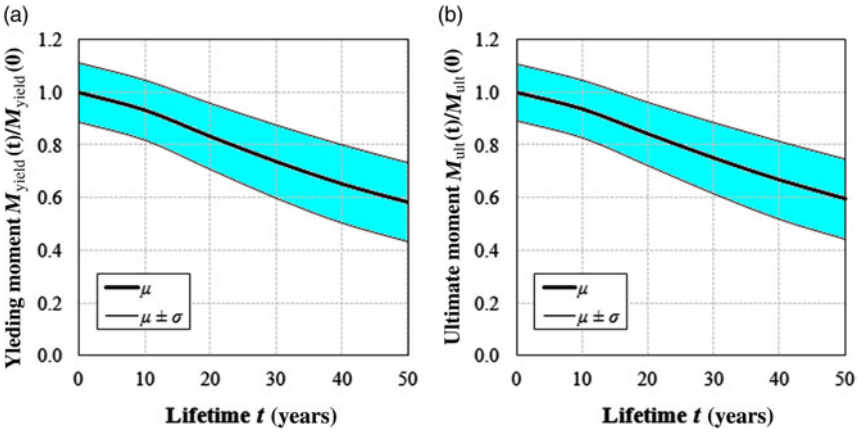

Figure 8. Time evolution of the structural performance of the pier cross-section in terms of (a) yielding moment $M_{yield}(t)$ and (b) ultimate moment $M_{ult}(t)$ (mean μ and standard deviation σ from the mean).

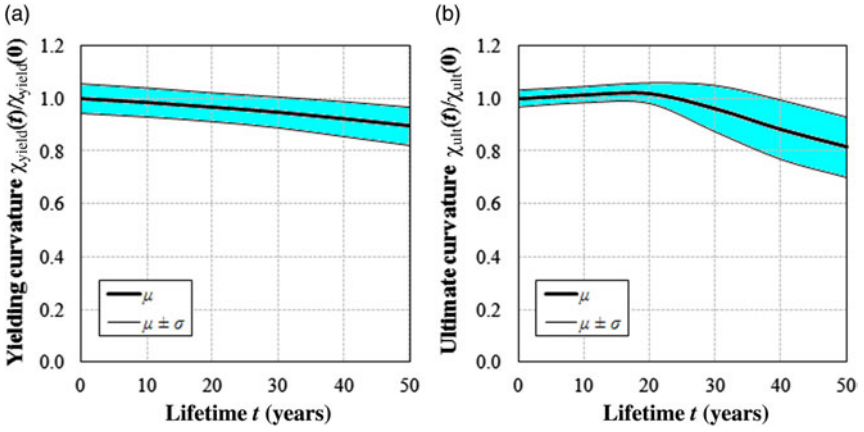

Figure 9. Time evolution of the structural performance of the pier cross-section in terms of (a) yielding curvature $\chi_{yield}(t)$ and (b) ultimate curvature $\chi_{ult}(t)$ (mean μ and standard deviation σ from the mean).

may depend with large uncertainty on the degradation of both concrete and steel properties.

The lifetime evolution of bending strength and curvature ductility obtained using the proposed approach well agrees with the results reported by Biondini et al. (2010), where the time-variant performance of the cross-section pier was investigated by means of a more general 2D diffusion modelling based on cellular automata (Biondini et al., 2004, 2006).

Lifetime seismic performance of concrete bridge structures

The global effects of the local damage phenomena on the overall seismic performance of bridge structures are investigated. As a case study, the four-span geometrically regular continuous bridge shown in Figure 11(a) is considered. Similar bridge structural schemes with irregular geometry have been investigated in Biondini

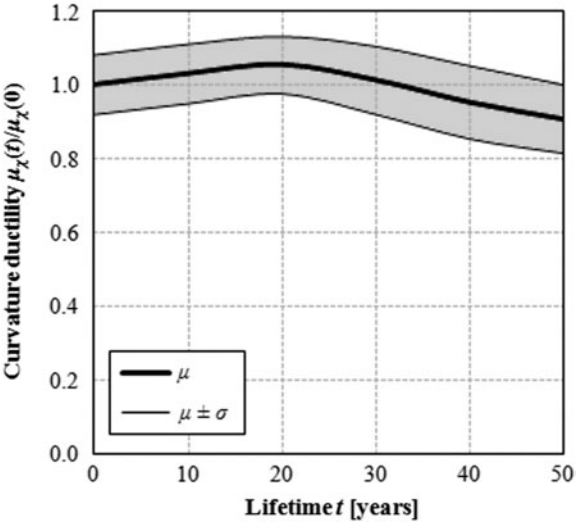

Figure 10. Time evolution of the structural performance of the pier cross-section in terms of curvature ductility $\mu_\chi(t)$ (mean μ and standard deviation σ from the mean).

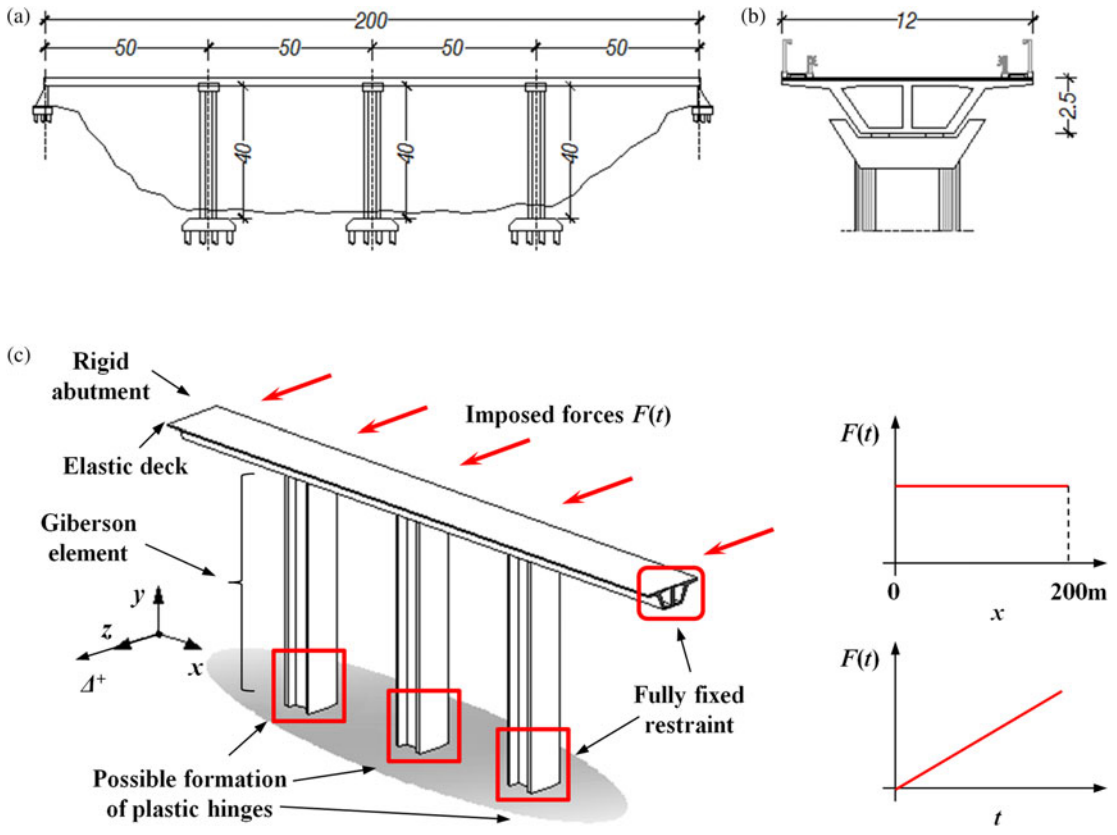

Figure 11. Bridge structure: (a) overall dimensions (in metres) and (b) deck cross-section at midspan; (c) structural modelling and applied push-over forces.

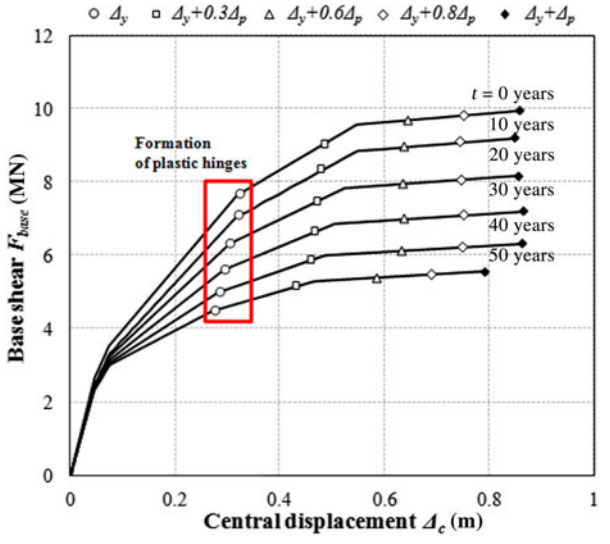

Figure 12. Push-over analyses based on the properties of the piers shown in Figure 7. Time evolution of total base shear force F_{base} versus top displacement of the central pier Δ_c during the first 50 years of lifetime with indication of increasing levels of displacement according to Table 3.

et al. (2010). The total length of the bridge is 200 m, with spans of 50 m. The bridge deck is a two-box girder, as shown in Figure 11(b). The cross-section of the bridge piers is shown in Figure 3. Connections of the deck with both piers and abutments are monolithic. The structure is considered fully fixed at the abutments and at the base of the piers. The seismic analysis is carried out by assuming a uniform gravity load $p = 300$ kN/m, including self weight, dead loads and a 20% of live loads applied on the deck.

The model of the bridge is shown in Figure 11(c). The deck is modelled by elastic beam elements, since under transversal loading the nonlinear behaviour is expected to develop only in the piers (Priestley, Calvi, & Kowalsky,

Table 3. System displacement limits considering different structural performance levels.

Structural performance level	Qualitative description	System displacement limit
SP-1	Fully Operational	Δ_y
SP-2	Operational	$\Delta_y + 0.3\Delta_p$
SP-3	Life Safe	$\Delta_y + 0.6\Delta_p$
SP-4	Near collapse	$\Delta_y + 0.8\Delta_p$
SP-5	Collapse	$\Delta_y + \Delta_p$

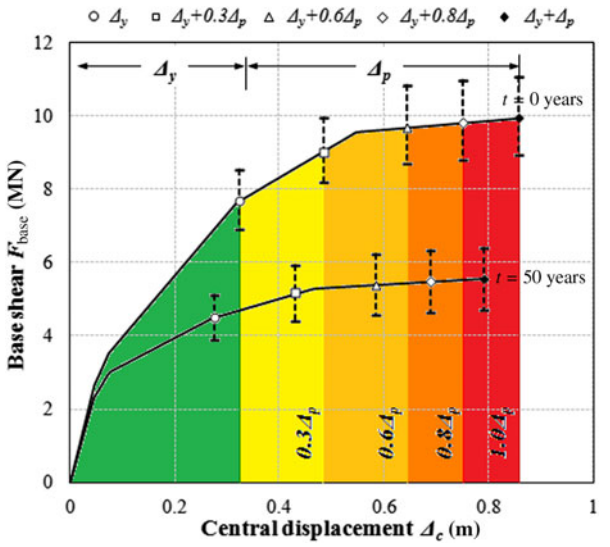

Figure 13. Push-over analyses. Total base shear force F_{base} versus top displacement of the central pier Δ_c at time $t = 0$ and $t = 50$ years with indication of the yielding Δ_y and plastic Δ_p displacements according to different levels of performance.

2007). The piers are modelled by using Giberson beam elements (Sharpe, 1974), with plastic hinges that can develop at top and bottom of the piers. Shear failures are excluded based on a proper capacity design. The flexural behaviour of the plastic hinges, which are modelled as rotational inelastic springs, is defined by moment-rotation relationships achieved by integration of the bending moment-curvature hysteresis rules. The integration is developed by assuming a parabolic distribution of the curvature along a fixed length region of the plastic hinge L_p. Before implementation, the bending moment-curvature relationships have been linearised, as shown in Figure 7(b). The main parameters of the model are the values of bending moment and curvature at cracking (M_{cr}, χ_{cr}), yielding (M_{yield}, χ_{yield}), peak (M_{max}, χ_{max}) and failure (M_{ult}, χ_{ult}). The cyclic behaviour of the plastic hinges is defined based on the Schoettler–Restrepo hysteresis rule (Carr, 2008).

Lifetime nonlinear static (push-over) analyses

A probabilistic lifetime nonlinear static (push-over) analysis of the bridge is carried out by using the program RUAUMOKO (Carr, 2008). A uniform distribution of monotonically increasing horizontal forces is applied at deck level, as suggested in CEN-EN 1998-1 (2004) due to the regular scheme of the bridge. Nonlinear geometrical $P - \Delta$ effects are not considered. Results of the lifetime push-over analyses assuming the mean properties of the bridge piers (Figure 7) are shown in Figure 12 in terms of total base shear force F_{base} versus top displacement of the central pier Δ_c. These diagrams show a significant decrease in the total base shear capacity of the bridge, which reduces to about 50% of the original value after 50 years of lifetime.

The points corresponding to the formation of the plastic hinges at the base of the central pier are highlighted on the push-over curves in Figure 12. As it can be noticed, in corroded structures the plastic hinging occurs for lower levels of displacement, which is mainly due to the reduced steel reinforcement area in concrete members.

The points corresponding to increasing displacement levels are also indicated on the push-over curves shown in Figure 12. As listed in Table 3, different seismic performance levels can be established according to the maximum displacement that the structure undergoes during an earthquake. Performance-based design approaches have been developed for buildings (SEAOC, 1995), but less has been done for bridges (Mander & Basoz, 1999). Nevertheless, structural performance levels can be effectively identified for bridges as well with respect to the inelastic displacement demand ratio. The performance levels are listed in Table 3 with

Table 4. Push-over analyses. Lifetime evolution of total base shear force F_{base} for different structural performance levels according to Table 3 (normalised mean values μ and standard deviations σ from the mean).

			Lifetime					
SPL	F_{base}		0	10 years	20 years	30 years	40 years	50 years
SP-1	$F_y(t)/F_y(0)$	μ	1	0.939	0.847	0.760	0.684	0.624
		σ	0.106	0.107	0.117	0.128	0.134	0.136
SP-2	$F_{OP}(t)/F_{OP}(0)$	μ	1	0.936	0.839	0.744	0.659	0.590
		σ	0.109	0.111	0.124	0.138	0.149	0.153
SP-3	$F_{LS}(t)/F_{LS}(0)$	μ	1	0.935	0.837	0.742	0.657	0.588
		σ	0.110	0.112	0.125	0.139	0.149	0.152
SP-4	$F_{NC}(t)/F_{NC}(0)$	μ	1	0.942	0.850	0.753	0.666	0.596
		σ	0.098	0.101	0.118	0.138	0.148	0.150
SP-5	$F_{ult}(t)/F_{ult}(0)$	μ	1	0.936	0.840	0.746	0.661	0.591
		σ	0.108	0.110	0.123	0.137	0.149	0.153

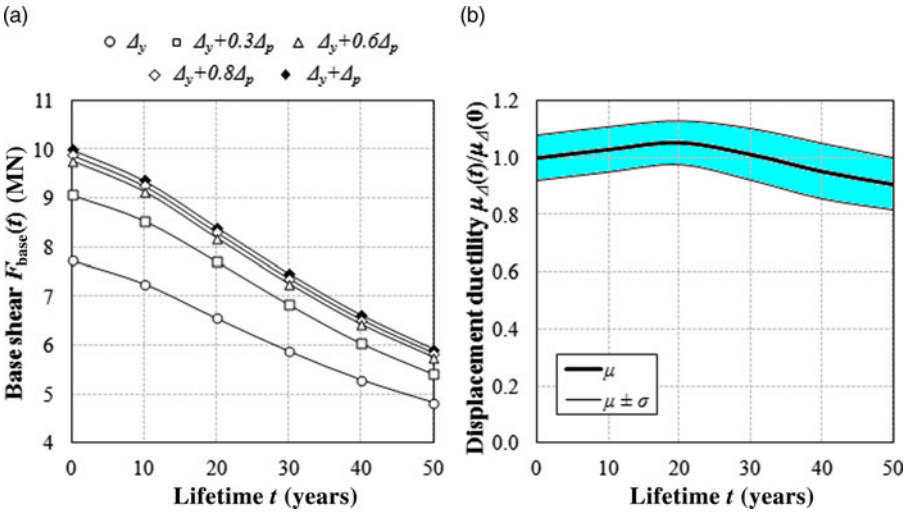

Figure 14. Push-over analyses. Time evolution of (a) mean total base shear force F_{base} with reference to different levels of displacement (see Figure 12) and (b) displacement ductility μ_Δ (mean values μ and standard deviation σ from the mean).

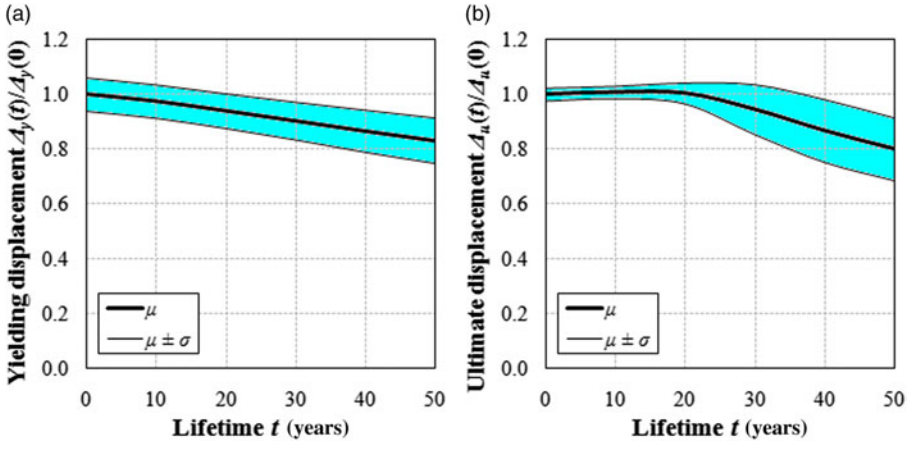

Figure 15. Push-over analyses. Time evolution of (a) yielding displacement Δ_y and (b) ultimate displacement Δ_u of the central pier (mean μ and standard deviation σ from the mean).

Table 5. Characteristics of the seismic records (Pampanin et al., 2002).

Earthquake record	Year	Station	Soil type	Scaling factor	Scaled PGA (g)
EQ1 – Loma Prieta	1989	Hollister Diff. Array	D	2.0	0.54
EQ2 – Loma Prieta	1989	Gilroy Array #7	D	3.0	0.68
EQ3 – Landers	1992	Desert Hot Springs	C	4.1	0.62
EQ4 – Landers	1992	Yermo Fire Station	D	3.3	0.50
EQ5 – Cape Mendocino	1992	Rio Dell Overpass-FF	C	1.8	0.69
EQ6 – Superstition Hills	1987	Plaster City	D	3.3	0.61
EQ7 – Northridge	1994	Canoga Park-Topanga Can	D	1.8	0.64
EQ8 – Northridge	1994	Beverly Hills 14145 Mulhol	C	1.4	0.56
EQ9 – Northridge	1994	N Holliwood-Coldwater Can	C	2.6	0.69
EQ10 – Northridge	1994	Sunland-Mt. Gleason Ave	C	3.3	0.52

Table 6. Recommended design ground motions for use in high seismic regions, with indication of PGAs (in units of g's) for sites not located in near source zones, soil type B (SEAOC, 1995).

Earthquake	Description	Probability of exceedance	Mean return period	PGA
EQ-I	Frequent	87%/50 years	25 years	0.11
EQ-II	Occasional	50%/50 years	72 years	0.17
EQ-III	Rare	–	250 to 800 years	0.40
EQ-IV	Maximum considered	–	800 to 2500 years	0.60

reference to the yielding displacement Δ_y of the bridge, i.e. the displacement at which the central pier reaches its yielding, and the plastic displacement $\Delta_p = \Delta_u - \Delta_y$, being Δ_u the displacement at which the central pier reaches its ultimate capacity. If the structure remains elastic, the bridge does not suffer any damage, and it can be declared 'fully operational' as soon after the seismic event. If the elastic limit is exceeded, then an increasing inelastic demand is placed to the structure as far as the maximum displacement of the structure increases until collapse. As a consequence, the bridge undergoes increasing damage with the increase in the plastic demand. Different performance levels can be qualitatively identified as 'operational', with limitation to traffic, 'life-safe', 'near collapse' and 'collapse', with evidence of their meaning, in order to classify the reduced post-earthquake performance of the structure.

Each of these structural performance levels can be identified as the objective of a performance-based design. In fact, for a prescribed displacement level the push-over curve provides the total resisting force of the bridge piers and hence the maximum peak ground acceleration

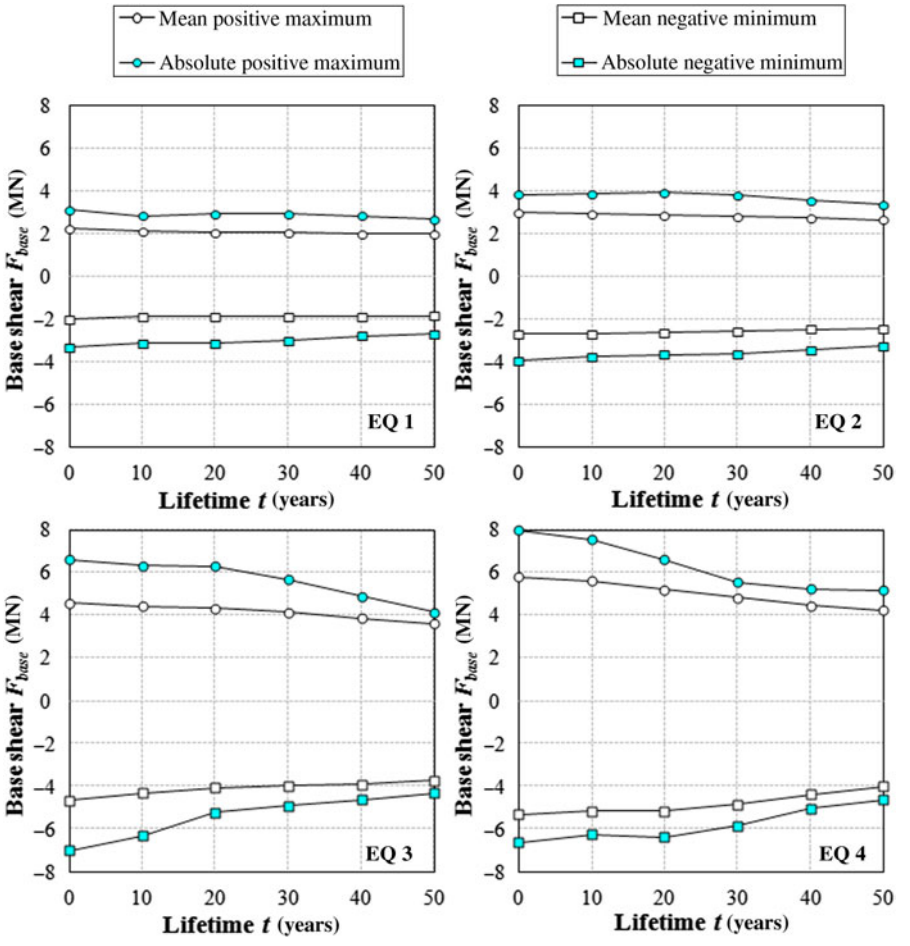

Figure 16. Time-history analyses. Time evolution of total base shear force F_{base} based on the properties of the piers shown in Figure 7 considering increasing levels of PGA (Table 6).

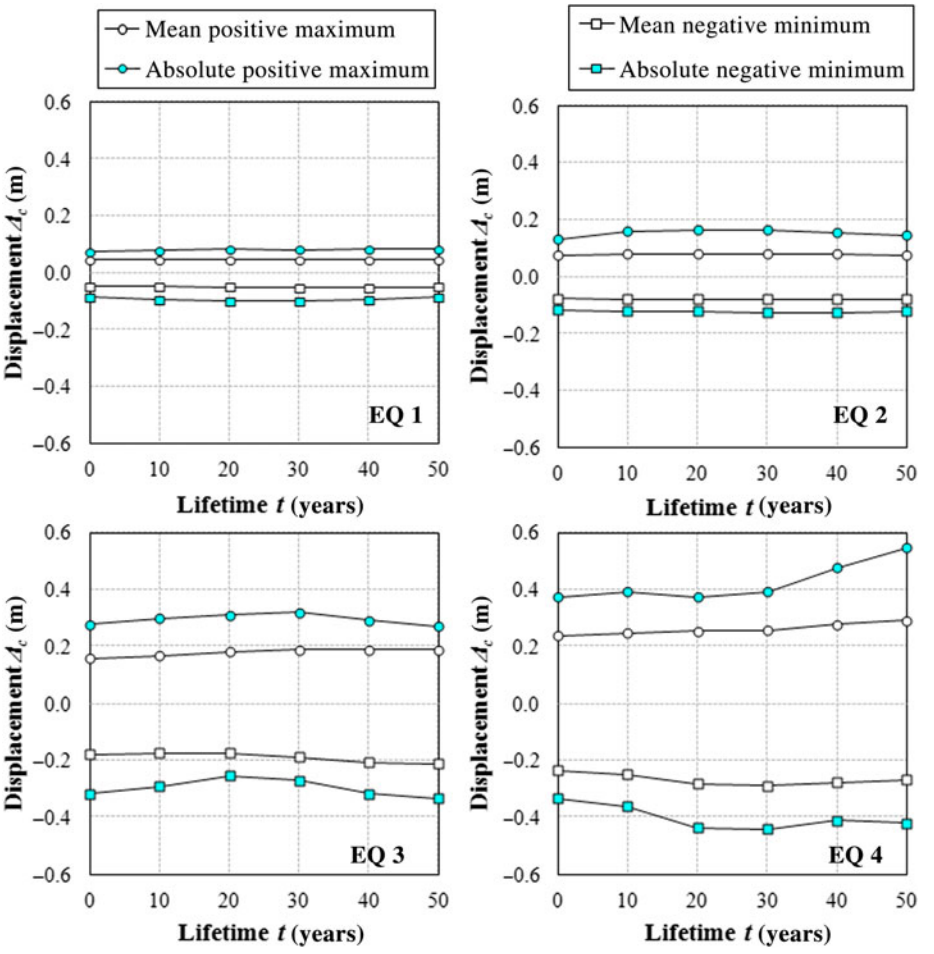

Figure 17. Time-history analyses. Time evolution of central pier top displacement Δ_c based on the properties of the piers shown in Figure 7 considering increasing levels of PGA (Table 6).

sustainable by the structure within a specified performance level. As it can be noticed from Figure 12, for each performance level, a progressive decrease in the strength capacity of the structure occurs as the corrosion of concrete members becomes more severe, which implies that after 50 years the structure could not sustain an earthquake event of the same magnitude it was designed for. This is evident in Figure 13, where the push-over curves at the beginning of lifetime and after 50 years are compared.

Since a shift of the yielding and ultimate displacement occurs in time, the seismic performance of a deteriorating bridge, evaluated in terms of displacements on the basis of the initial properties of the structure, may not comply with the prescribed target performance levels over the expected lifetime. Moreover, the uncertainties associated with each performance level in terms of total base shear are different, as shown by dotted lines in Figure 13, which represent the dispersion of the results around the mean shear value. Results of the probabilistic analyses are listed in Table 4, in terms of normalised mean values and standard deviations of the total base shear throughout the lifetime. It can be noticed that the dispersion of the results around the mean becomes greater not only as the age of the structure increases, but also, in general, considering increasing levels of performance.

Figure 14(a) shows the lifetime evolution of the total base shear $F_{base}(t)$ at different structural performance levels. For example, the total base shear $F_{base}(t)$ at ultimate displacement Δ_u of the structure decreases of about 40% during a 50-year lifetime. Base shear forces at intermediate displacement levels from yielding displacement up to collapse decrease as well proportionately. The displacement ductility of the structural system $\mu_\Delta(t) = \Delta_u(t)/\Delta_y(t)$ may change as well, as shown in Figure 14(b), since the reduction in steel area and the degradation of concrete strength in the corroded members vary the distribution of stiffness in the structure. As a consequence, a change in the global collapse mechanism and a performance decay of the bridge may occur.

Table 7. Time-history analyses. Lifetime evolution of (a) total base shear force F_{base} and (b) central pier top displacement Δ_c for increasing levels of seismic demand, according to Table 6.

		Lifetime					
Earthquake	F_{base} (kN)	0 years	10 years	20 years	30 years	40 years	50 years
(a)							
EQ-I	Absolute max	3.120 (6)	2.840 (6)	2.938 (2)	2.949 (2)	2.845 (2)	2.695 (2)
	Mean max	2.249	2.134	2.088	2.056	2.025	1.992
	Mean min	−1.980	−1.880	−1.875	−1.873	−1.854	−1.839
	Absolute min	−3.302 (2)	−3.116 (2)	−3.104 (2)	−2.986 (2)	−2.783 (2)	−2.678 (2)
EQ-II	Absolute max	3.842 (2)	3.894 (2)	3.951 (2)	3.802 (2)	3.575 (2)	3.358 (2)
	Mean max	2.980	2.929	2.886	2.810	2.737	2.660
	Mean min	−2.693	−2.680	−2.635	−2.568	−2.469	−2.433
	Absolute min	−3.949 (2)	−3.762 (2)	−3.650 (2)	−3.596 (2)	−3.421 (2)	−3.253 (2)
EQ-III	Absolute max	6.621 (7)	6.334 (2)	6.298 (2)	5.669 (2)	4.890 (2)	4.135 (2)
	Mean max	4.579	4.439	4.337	4.138	3.844	3.588
	Mean min	−4.662	−4.340	−4.082	−3.980	−3.924	−3.732
	Absolute min	−7.028 (7)	−6.305 (7)	−5.228 (7)	−4.919 (7)	−4.639 (7)	−4.332 (3)
EQ-IV	Absolute max	7.980 (2)	7.549 (2)	6.623 (2)	5.539 (7)	5.251 (3)	5.180 (3)
	Mean max	5.785	5.598	5.194	4.830	4.452	4.230
	Mean min	−5.322	−5.166	−5.169	−4.861	−4.394	−4.024
	Absolute min	−6.619 (7)	−6.280 (3)	−6.383 (3)	−5.854 (3)	−5.051 (2)	−4.617 (2)

		Lifetime					
Earthquake	Δ_c (m)	0 years	10 years	20 years	30 years	40 years	50 years
(b)							
EQ-I	Absolute max	0.075 (2)	0.081 (2)	0.084 (2)	0.082 (3)	0.083 (3)	0.083 (3)
	Mean max	0.047	0.047	0.047	0.047	0.047	0.047
	Mean min	−0.047	−0.048	−0.049	−0.050	−0.050	−0.049
	Absolute min	−0.085 (2)	−0.092 (2)	−0.097 (2)	−0.098 (2)	−0.092 (2)	−0.083 (2)
EQ-II	Absolute max	0.131 (2)	0.157 (2)	0.165 (2)	0.163 (2)	0.156 (2)	0.145 (2)
	Mean max	0.073	0.078	0.079	0.079	0.078	0.076
	Mean min	−0.078	−0.080	−0.081	−0.080	−0.080	−0.081
	Absolute min	−0.117 (2)	−0.123 (2)	−0.123 (2)	−0.126 (2)	−0.128 (2)	−0.124 (2)
EQ-III	Absolute max	0.278 (7)	0.297 (7)	0.311 (2)	0.321 (2)	0.292 (2)	0.271 (3)
	Mean max	0.159	0.168	0.182	0.189	0.189	0.188
	Mean min	−0.178	−0.175	−0.174	−0.188	−0.208	−0.213
	Absolute min	−0.318 (7)	−0.293 (7)	−0.255 (7)	−0.271 (3)	−0.317 (3)	−0.333 (3)
EQ-IV	Absolute max	0.373 (2)	0.391 (2)	0.373 (2)	0.392 (3)	0.476 (3)	0.546 (3)
	Mean max	0.237	0.248	0.254	0.258	0.277	0.292
	Mean min	−0.234	−0.249	−0.281	−0.289	−0.276	−0.269
	Absolute min	−0.334 (7)	−0.362 (3)	−0.438 (3)	−0.443 (3)	−0.410 (2)	−0.420 (2)

Note: Numbers in parentheses refer to the earthquake numbers listed in Table 5.

The time-variant trend of both mean and standard deviation of displacement ductility results from the combination of the variability of both yielding and ultimate displacement, as shown in Figure 15. In fact, while the yielding displacement $\Delta_y(t)$ decreases monotonically, the trend of the ultimate displacement $\Delta_u(t)$ is similar to that of the ultimate curvature $\chi_{ult}(t)$ (Figure 9). Moreover, larger uncertainties affect the behaviour of the bridge at collapse, especially after 25 years of lifetime, while the transition from elastic to plastic field is mainly related to the properties of the reinforcing steel bars only. This result confirms that at the design stage higher safety factors should be applied to check the ultimate deformation capacity of the bridge with respect to the safety factors used to check the reaching of the yielding displacement.

Lifetime nonlinear dynamic analyses

Time-history nonlinear dynamic analyses are carried out with reference to the ensemble of 10 earthquake records listed in Table 5 (Pampanin, Christopoulos, & Priestley, 2002). These records were selected to match the Eurocode 8 design response spectrum for soil class B and peak ground acceleration PGA = 0.54 *g* (CEN-EN 1998-1, 2004). In this study, the records are scaled to prescribed seismic intensity levels, corresponding to frequent, occasional, rare and maximum considered

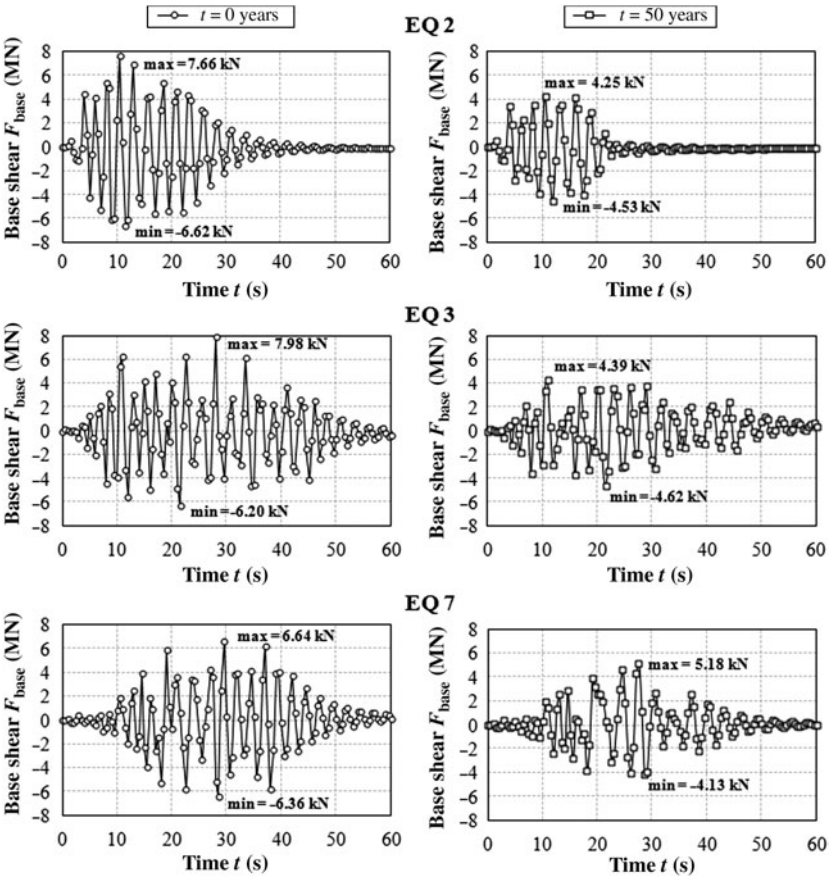

Figure 18. Time-history analyses. Time histories of total base shear F_{base} at time $t = 0$ and $t = 50$ years for three of the earthquakes listed in Table 5.

ground motions, as listed in Table 6 (SEAOC, 1995). These ground motions have increasing mean return periods, ranging from a 25-year to a 2500-year return period, thus corresponding to an increasing seismic hazard. The investigation is therefore focused on the effects of increasing seismicity on corroded structures under the same environmental exposure. Further analyses should be required to combine different levels of environmental aggressiveness and seismic hazard (Biondini et al., 2012).

The dynamic analyses are carried out on the bridge model considering the mean values of the bending moment-curvature diagrams of the box cross-section bridge pier shown in Figure 7. Results are reported in terms of mean and absolute maxima/minima values of total base shear F_{base} (Figure 16) and top displacement of the central pier Δ_c (Figure 17). As expected based on the results of the push-over analyses, these parameters vary depending not only on the seismic intensity level but also on the age of the structure. The influence of the ageing phenomena in concrete is more evident with the increase in the peak ground acceleration in terms of both base shear force and displacement demand. Since the concrete members become less stiff over lifetime, the total shear at the base of the bridge piers decreases, while the displacement demand at deck level increases. This trend is clearly indicated by the mean values of forces and displacements shown in Figures 16 and 17, respectively. The curves related to the maxima/minima values are less smooth than the curves of the mean values due to the inherent randomness of the considered seismic excitations acting on the structure.

The results of the time-history analyses are also listed in Table 7, with indication of the earthquake records associated with absolute maximum/minimum values of base shear force F_{base} and central pier top displacement Δ_c. In particular, it can be noticed that the maximum/minimum displacement at the beginning of the lifetime is generally due to the ground motions with higher peak ground acceleration (e.g. EQ7). On the contrary, at the end of the lifetime, the observed major displacements are reached for the seismic events with longer durations (e.g. EQ2 and EQ3). This can be due to the developing of the degradation phenomena, since the structure becomes

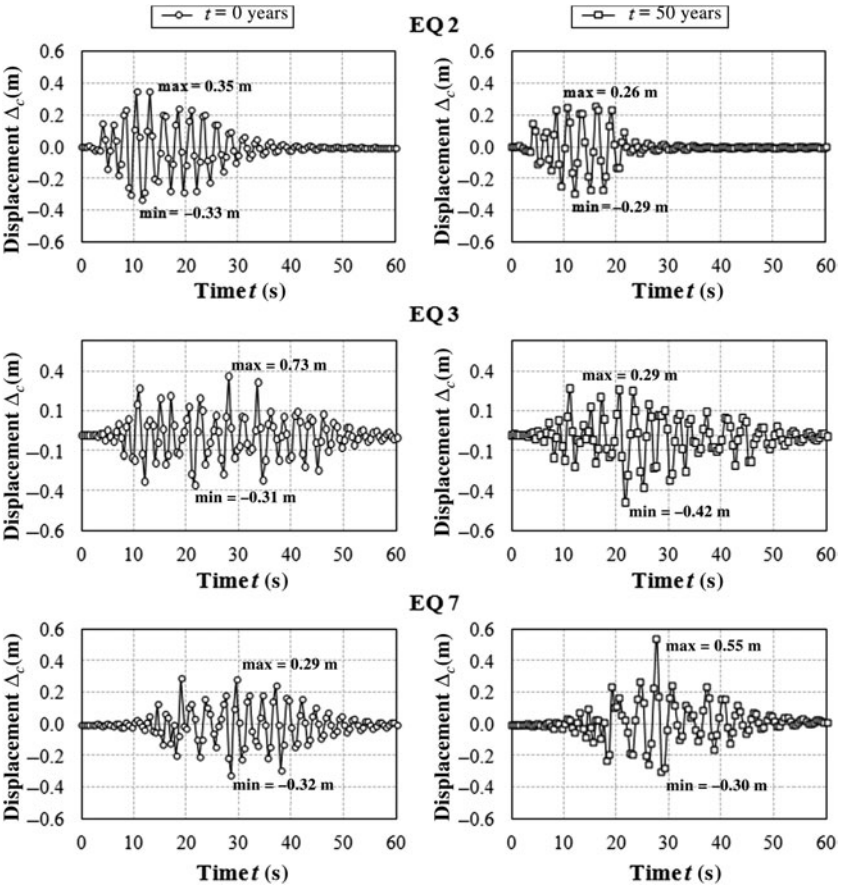

Figure 19. Time-history analyses. Time histories of central pier top displacement Δ_c at time $t = 0$ and $t = 50$ years for three of the earthquakes listed in Table 5.

less stiff and more ductile between 10 and 30 years of lifetime (Figure 14(b)).

According to the results of the time-histories analyses, the trend shown by the push-over analyses is confirmed. In fact, considering the major seismic intensity 'Level IV', at time $t = 0$ the maximum base force is about 7 MN, while the maximum displacement is between 0.2 and 0.4 m. This indicates an elastic response of the structure, which is expected to remain operational after the earthquake. On the contrary, after 50 years of lifetime the most severe seismic input places a demand of 5 MN of base shear and of $\sim$0.6 m of maximum displacement. These data correspond to a point in the 'near collapse' zone on the push-over curve at $t = 50$ years in Figure 12.

Finally, time histories of total base shear F_{base} and top displacement of the central pier Δ_c are shown in Figures 18 and 19, respectively, for three of the earthquakes listed in Table 5 (EQ2, EQ3 and EQ7). These results refer to time instants $t = 0$ and $t = 50$ years. It can be noticed that over the lifetime the overall strength of the bridge decreases and the displacement demand increases, due to the reduced stiffness of the corroded concrete piers. This could cause an unsatisfactory structural performance of a bridge that was designed to respect prescribed performance levels at the beginning of its lifetime.

Conclusions

The effects of chloride induced corrosion of steel reinforcement and degradation of concrete on the lifetime seismic performance of bridges have been investigated. The proposed probabilistic procedure allowed to model the degradation process into concrete members at cross-sectional level and hence to evaluate their lifetime performance in terms of both bending moment resistance and curvature ductility. The global effects of the local damage phenomena on the overall seismic performance have been therefore investigated with reference to a continuous bridge structure. The results showed that the variation of the pier flexural strength and ductility could significantly affect the overall response of the bridge structure under seismic excitation, since, in general, the seismic performance of integral bridges strictly depends on the capacity of the piers. As a consequence, the global

behaviour of the bridge system varies during lifetime involving a significant reduction of the base shear strength and a variation of the displacement ductility.

A design targeted to satisfy certain performance levels in terms of forces or displacements, as stated by recent performance-based design codes, could hence become unsatisfactory throughout the lifetime of the structure whether considering the residual capacity of concrete members. In fact, a redistribution of the stiffness and a variation in the resisting hierarchy, which eventually cause a shift to an undesirable mechanism of collapse, may occur, especially if the corrosion phenomena are localised in certain parts of the structure.

Within this scenario, the results demonstrated the importance of taking the severity of the environmental exposure and the required structural lifetime into account in the seismic design of structures. Therefore, the design criteria should be revised since the performance of ageing bridges reduces over time. New generation performance-based design procedures should be developed by using a performance matrix in which the structural behaviour is related not only to the seismic intensity level but also to the environmental hazard, taking into account increasing levels of aggressiveness.

Based on that, a proper calibration of the design objectives should also be planned in order to ensure a structural lifetime with suitable levels of performance, from fully operational to collapse. In this regard, further investigation about the interaction between seismic and corrosion hazards would be needed to properly define a life cycle-oriented performance-based design approach for new bridges and to plan seismic assessment strategies for existing bridges.

References

Akiyama, M., & Frangopol, D.M. (2010). On life-cycle reliability under earthquake excitations of corroded reinforced concrete structures. *Proceedings of the Second International Symposium on Life-Cycle Civil Engineering, (IALCCE2010)*, Taipei, Taiwan, October 27–31.

Akiyama, M., Frangopol, D.M., & Matsuzaki, H. (2011a). Life-cycle reliability of RC bridge piers under seismic and airborne chloride hazards. *Earthquake Engineering and Structural Dynamics*, *40*(15), 1671–1687.

Akiyama, M., Frangopol, D.M., & Suzuki, M. (2011b). Integration of the effects of airborne chlorides into reliability-based durability design of reinforced concrete structures in a marine environment. *Structure and Infrastructure Engineering*, *8*(2), 125–134.

Akiyama, M., Matsuzaki, H., Dang, H.T., & Suzuki, M. (2012). Reliability-based capacity design for reinforced concrete bridge structures. *Structure and Infrastructure Engineering*, *8*(12), 1096–1107.

Alipour, A., Shafei, B., & Shinozuka, M.S. (2013). Capacity loss evaluation of reinforced concrete bridges located in extreme chloride-laden environments. *Structure and Infrastructure Engineering*, *9*(1), 8–27.

Almusallam, A. (2001). Effect of degree of corrosion on the properties of reinforcing steel bars. *Construction and Building Materials*, *15*, 361–368.

Alonso, C., Andrade, C., Castellote, M., & Castro, P. (2000). Chloride threshold values to depassivate reinforcing bars embedded in a standardized OPC mortar. *Cement and Concrete Research*, *30*, 1047–1055.

Alonso, C., Andrade, J., Rodriguez, J., & Diez, J.M. (1998). Factors controlling cracking of concrete affected by reinforcement corrosion. *Materials and Structures*, *31*, 435–441.

Alonso, C., Castellote, M., & Andrade, C. (2002). Chloride threshold dependence of pitting potential of reinforcements. *Electrochimica Acta*, *47*, 3459–3481.

Andrade, C., & Alonso, M.C. (1994). Values of corrosion rate of steel in concrete to predict service life of concrete structures. In G. Cragnolino & N. Sridhar (Eds.), *Application of accelerated corrosion tests to service life prediction of materials, ASTM STP 1194* (pp. 29–37). Philadelphia, PA: American Society for Testing and Materials.

Andrade, C., Alonso, M.C., & Gonzalez, J.A. (1990). An initial effort to use the corrosion rate measurement for estimating rebar durability. In N.S. Berke, V. Chaker, & D. Whinting (Eds.), *Corrosion rates of steel in concrete, ASTM STP 1065* (pp. 29–37). Philadelphia, PA: American Society for Testing and Materials.

Apostolopoulos, C.A., & Papadakis, V.G. (2008). Consequences of steel corrosion on the ductility properties of reinforcement bar. *Construction and Building Materials*, *22*, 2316–2324.

Berto, L., Vitaliani, R., Saetta, A., & Simioni, P. (2009). Seismic assessment of existing RC structures affected by degradation phenomena. *Structural Safety*, *31*, 284–297.

Bertolini, L., Elsener, B., Pedeferri, P., & Polder, R. (2004). *Corrosion of steel in concrete – Prevention, diagnosis, repair.* Weinheim: Wiley-VCH.

Biondini, F. (2011). Cellular automata simulation of damage processes in concrete structures. In Y. Tsompanakis & B.H. V. Topping (Eds.), *Soft computing methods for civil and structural engineering*, Chapter 10 (pp. 229–264). Stirlingshire: Saxe-Coburg Publications.

Biondini, F., Camnasio, E., & Palermo, A. (2010). Lifetime seismic performance of concrete bridges. *Proceedings of the Fifth International Conference on Bridge Maintenance, Safety, and Management (IABMAS2010)*, Philadelphia, PA, July 11–15. In: *Bridge Maintenance, Safety, Management and Life-cycle Optimization*, D.M. Frangopol, R. Sause, C. S. Kusko (Eds.), CRC Press, Taylor & Francis Group.

Biondini, F., Camnasio, E., & Palermo, A. (2012). Life-cycle performance of concrete bridges exposed to corrosion and seismic hazard. *Proceedings of the Structures Congress 2012 (ASCE2012)*, Chicago, IL, March 29–31.

Biondini, F., Bontempi, F., Frangopol, D.M., & Malerba, P.G. (2004). Cellular automata approach to durability analysis of concrete structures in aggressive environments. *Journal of Structural Engineering, ASCE*, *130*(11), 1724–1737.

Biondini, F., Bontempi, F., Frangopol, D.M., & Malerba, P.G. (2006). Probabilistic service life assessment and maintenance planning of concrete structures. *Journal of Structural Engineering, ASCE*, *132*(5), 810–825.

Biondini, F., & Frangopol, D.M. (2008a). Probabilistic limit analysis and lifetime prediction of concrete structures. *Structure and Infrastructure Engineering*, *4*(5), 399–412.

Biondini, F. & Frangopol, D.M. (Eds.). (2008b). *Life-cycle civil engineering*. London: CRC Press, Taylor & Francis Group.

Biondini, F., Palermo, A., & Toniolo, G. (2011). Seismic performance of concrete structures exposed to corrosion: Case studies of low-rise precast buildings. *Structure and Infrastructure Engineering*, *7*(1–2), 109–119.

Biondini, F., & Vergani, M. (2012). Damage modeling and nonlinear analysis of concrete bridges under corrosion. *Proceedings of the Sixth International Conference on Bridge Maintenance, Safety and Management (IABMAS 2012)*, Stresa, Italy, July 8-12. In: *Bridge Maintenance, Safety, Management, Resilience and Sustainability*, F. Biondini, D. M. Frangopol (Eds.), CRC Press, Taylor and Francis Group.

Browne, R.D., Geoghegan, M.P., & Baker, A.F. (1983). *Corrosion of reinforcements in concrete construction* (A.P. Crane Ed.), (pp. 193–222). London: Ellis Hordwood Ltd.

Carr, A.J. (2008). *RUAUMOKO program for inelastic dynamic analysis*. Christchurch, New Zealand: Department of Civil Engineering, University of Canterbury.

CEB (1992). Durable Concrete Structures – Design Guide. *Bulletin*, *183*.

CEN-EN 1998-1 (2004). *Eurocode 8: Design of structures for earthquake resistance. Part 1: General rules, seismic actions and rules for buildings*. Brussels: European Committee for Standardization.

Choe, D., Gardoni, P., Rosowsky, D., & Haukaas, T. (2008). Probabilistic capacity models and seismic fragility estimates for RC columns subject to corrosion. *Reliability Engineering and System Safety*, *93*(3), 383–393.

Choe, D., Gardoni, P., Rosowsky, D., & Haukaas, T. (2009). Seismic fragility estimates for reinforced concrete bridges subject to corrosion. *Structural Safety*, *31*, 275–283.

Coronelli, D., & Gambarova, P. (2004). Structural assessment of corroded reinforced concrete beams: Modeling guidelines. *Journal of Structural Engineering*, ASCE, *130*(8), 1214–1224.

Estes, A.C., & Frangopol, D.M. (2001). Bridge lifetime system reliability under multiple limit states. *Journal of Bridge Engineering*, *6*(6), 523–528.

fib (2006). Model Code for Service Life Design. *Bulletin*, *34*.

Ghosh, J., & Padgett, J.E. (2009). Multi-hazards considerations of seismic and aging threats to bridges. *Proceedings of the SEI/ASCE Structures Congress 2009*, Austin, TX, USA, April 30 – May 2.

Ghosh, J., & Padgett, J.E. (2010). Aging considerations in the development of time-dependent seismic fragility curves. *ASCE Journal of Structural Engineering*, *136*(12), 1497–1511.

Glass, G.K., & Buenfeld, N.R. (1997). The presentation of the chloride threshold level for corrosion of steel in concrete. *Corrosion Science*, *39*(5), 1001–1013.

Glicksman, M.E. (2000). *Diffusion in solids*. New York, NY: John Wiley & Sons.

Hamada, M. (1968). Properties of paste and concrete. *Proceedings of the Fifth International Symposium on the Chemistry of Cement*, Part III, Vol. III, Tokyo, Japan, 344–369.

Hope, B.B., & Alan, K.C.Ip. (1987). Chloride corrosion threshold in concrete. *ACI Materials Journal*, *84*, 306–314.

Kobayashi, K. (2006). The seismic behavior of RC members suffering from chloride-induced corrosion. *Proceedings of the Second fib Congress*, Naples, Italy, June 5–8.

Kumar, R., Gardoni, P., & Sanchez-Silva, M. (2009). Effect of cumulative seismic damage and corrosion on the life cycle cost of reinforced concrete bridges. *Earthquake Engineering and Structural Dynamics*, *38*, 887–905.

Liu, T., & Weyers, R.W. (1998). Modeling the dynamic corrosion process in chloride contaminated structures. *Cement and Concrete Research*, *28*(3), 365–379.

Malerba, P.G. (Ed.). (1998). *Limit and nonlinear analysis of reinforced concrete structures*. Udine: International Centre for Mechanical Sciences (CISM) (in Italian).

Mander, J.B., & Basoz, N. (1999). Seismic fragility curve theory for highway bridges in transportation lifeline loss estimation. *Optimizing post-earthquake lifeline system reliability*, TCLEE monograph no. 16 (Vol. 59) (pp. 315–338). Reston, VA: American Society of Civil Engineering and Design 1980.

Naito, H., Akiyama, M., & Suzuki, M. (2011). Ductility evaluation of concrete-encased steel bridge piers subjected to lateral cyclic loading. *Journal of Bridge Engineering*, *16*(1), 72–81.

Ou, Y.-C.O., Tsai, L-L.T., & Chen, H.-H. (2012). Cyclic performance of large-scale corroded reinforced concrete beams. *Earthquake Engineering and Structural Dynamics*, *41*(4), 593–604.

Ou, Y.-C., Wang, P.-H., Tsai, M.-S., Chang, K-C., & Lee, G.C. (2010). Large-scale experimental study of precast segmental unbonded post-tensioned concrete bridge columns for seismic regions. *Journal of Structural Engineering*, ASCE, *136*(3), 255–264.

Oyado, M., Saito, Y., Yasojima, A., Kanakubo, T., & Yamamoto, Y. (2007). Structural performance of corroded RC column under seismic load. *Proceedings of the First International Workshop on Performance, Protection and Strengthening of Structures under Extreme Loading*, Whistler, Canada, August 20–22.

Palermo, A., & Pampanin, S. (2008). Enhanced seismic performance of hybrid bridge systems: Comparison with traditional monolithic solutions. *Journal of Earthquake Engineering*, *12*(8), 1267–1295.

Pampanin, S., Christopoulos, C., & Priestley, M.J.N. (2002). *Residual deformations in the performance-based seismic assessment of frame structures*. Pavia: IUSS Press.

Park, R., & Paulay, T. (1975). *Reinforced concrete structures*. New York: John Wiley & Sons.

Papia, M., Russo, G., & Zingone, G. (1988). Instability of longitudinal bars in RC columns. *Journal of Structural Engineering*, ASCE, *114*(2), 445–461.

Pastore, T., & Pedeferri, P. (1994). La Corrosione e la Protezione delle Opere Metalliche Esposte all'Atmosfera. *L'edilizia*, December, 75–92 (in Italian).

Priestley, M.J.N., Calvi, G.M., & Kowalsky, M.J. (2007). *Displacement-based seismic design of structures*. Pavia: IUSS Press.

Saito, Y., Oyado, M., Kanakubo, T., & Yamamoto, Y. (2007). Structural performance of corroded RC column under uniaxial compression load. *Proceedings of the First International Workshop on Performance, Protection & Strengthening of Structures under Extreme Loading*, Whistler, Canada, August 20–22.

SEAOC Vision 2000 Committee (1995). *Performance based seismic engineering*. Sacramento, CA: Structural Engineers Associate of California.

Sharpe, R.D. (1974). *The seismic response of inelastic structures* (PhD Thesis). Christchurch, New Zealand: Department of Civil Engineering, University of Canterbury.

Stewart, M.G. (2009). Mechanical behavior of pitting corrosion of flexural and shear reinforcement and its effect on structural reliability of corroding RC beams. *Structural Safety*, *31*, 19–30.

Thoft-Christensen, P. (1998). Assessment of the reliability profiles for concrete bridges. *Engineering Structures*, *20*(11), 1004–1009.

Val, D.V., Stewart, M.G., & Melchers, R.E. (1998). Effect of reinforcement corrosion on reliability of highway bridges. *Engineering Structures*, *20*, 1010 – 1019.

Vergani, M. (2010). *Damage modeling of concrete structures subject to corrosion* (Master Degree Thesis). Politecnico di Milano, Italy (in Italian).

Vidal, T., Castel, A., & Francois, R. (2004). Analyzing crack width to predict corrosion in reinforced concrete. *Cement and Concrete Research*, *34*, 165 – 174.

Yamamoto, T., Hattori, A., & Miyagawa, T. (2006). Uniaxial compression behavior of confined concrete deteriorated by corrosion of reinforcing steel. *Journal of the Society of Material Science*, *55*(10), 911 – 916 (in Japanese).

Zhang, R., Castel, A., & François, R. (2009). The corrosion pattern of reinforcement and its influence on serviceability of reinforced concrete members in chloride environment. *Cement and Concrete Research*, *39*(11), 1077 – 1086.